Neuron
Article

High-Frequency Organization and Synchrony of Activity in the Purkinje Cell Layer of the Cerebellum

Camille de Solages,[1] Germán Szapiro,[1] Nicolas Brunel,[2] Vincent Hakim,[3] Philippe Isope,[1] Pierre Buisseret,[4] Charly Rousseau,[1] Boris Barbour,[1] and Clément Léna[1,*]
[1]Laboratoire de Neurobiologie, UMR 8544, École Normale Supérieure, 46 rue d'Ulm, 75005 Paris, France
[2]Laboratoire de Neurophysique et Physiologie, UMR 8119, Université René Descartes, 45 rue des Saints Pères, 75006 Paris, France
[3]Laboratoire de Physique Statistique, UMR 8550, École Normale Supérieure, 24 rue Lhomond 75005 Paris, France
[4]Département Régulation, Développement, Diversité moléculaire, Muséum national d'Histoire naturelle, 57 rue Cuvier, 75005 Paris, France
*Correspondence: lena@biologie.ens.fr
DOI 10.1016/j.neuron.2008.05.008

SUMMARY

The cerebellum controls complex, coordinated, and rapid movements, a function requiring precise timing abilities. However, the network mechanisms that underlie the temporal organization of activity in the cerebellum are largely unexplored, because in vivo recordings have usually targeted single units. Here, we use tetrode and multisite recordings to demonstrate that Purkinje cell activity is synchronized by a high-frequency (~200 Hz) population oscillation. We combine pharmacological experiments and modeling to show how the recurrent inhibitory connections between Purkinje cells are sufficient to generate these oscillations. A key feature of these oscillations is a fixed population frequency that is independent of the firing rates of the individual cells. Convergence in the deep cerebellar nuclei of Purkinje cell activity, synchronized by these oscillations, likely organizes temporally the cerebellar output.

INTRODUCTION

The cerebellum is involved in the learning and control of coordinated movements. The finesse and rapidity of such movements imply very precise timing abilities. Indeed, temporal accuracy has long been considered one of the hallmarks of cerebellar learning (Raymond et al., 1996; Christian and Thompson, 2003; De Zeeuw and Yeo, 2005). However, very little is known about how the cerebellar circuitry can generate such accurate timings, partly due to the paucity of simultaneous recordings of multiple neurons in the cerebellum; nearly all previous in vivo recordings from the cerebellum have sought isolated single Purkinje cells. Despite the rarity of multineuron cerebellar recordings, reports exist of two phenomena that reflect a precise temporal organization of cerebellar cortical activity: millisecond synchrony of Purkinje cell action potentials and high-frequency (~200 Hz) oscillations of the field potential.

Recordings of pairs of Purkinje cells have revealed a precise synchrony (~1 ms) between cells separated by less than 100 μm (Bell and Grimm, 1969; Ebner and Bloedel, 1981; Shin and De Schutter, 2006) or between functionally related Purkinje cells (De Zeeuw et al., 1997). This synchrony has been suggested to result from common parallel fiber input (Bell and Grimm, 1969), but this issue remains unresolved.

Fast oscillatory activity in the cerebellum was first observed by Adrian (Adrian, 1935; Isope et al., 2002) in the form of low-amplitude, high-frequency (150–250 Hz) oscillations in the mammalian cerebellar electroencephalogram in decerebrate and anesthetized preparations. These oscillations were subsequently reported in the cerebellar cortices of fish, amphibians, reptiles, and birds (reviewed in Brookhart, 1960). Later observations in chronically implanted mammals indicated that the oscillations increased in intensity during active waking and paradoxical sleep (Pellet et al., 1974). However, the relation between neuronal firing and the oscillations was not studied, and no satisfactory mechanism for these oscillations was established. Recently, a pathological form of these oscillations has been associated with cerebellar ataxia in several mutant mice (Cheron et al., 2004, 2008). Large-amplitude and large-scale field-potential oscillations were observed in the cerebellar cortices of these animals. Purkinje cells were phase locked to the oscillations, whose amplitude was largest in the Purkinje cell layer. This work thus suggests a link between Purkinje cells and the fast oscillations.

In the present study, we use cerebellar tetrode recordings in vivo to investigate the population dynamics of Purkinje cell activity. We confirm the existence of both high-frequency oscillation and precise synchrony and show that these two phenomena are directly related. Investigation of the underlying mechanisms allows us to exclude parallel fibers as necessary for either phenomenon, contrary to previous suggestions. Instead, we show how an inhibitory mechanism involving the recurrent axon collaterals of Purkinje cells can generate both oscillations and synchrony. Finally, we elucidate specific properties of the oscillations, which notably exhibit a fixed frequency independent of the Purkinje cell firing rate. Purkinje cells converge strongly upon deep cerebellar nuclear cells, so these oscillations and synchrony are likely to be impressed upon the cerebellar output neurons and therefore to organize the output from the cerebellum.

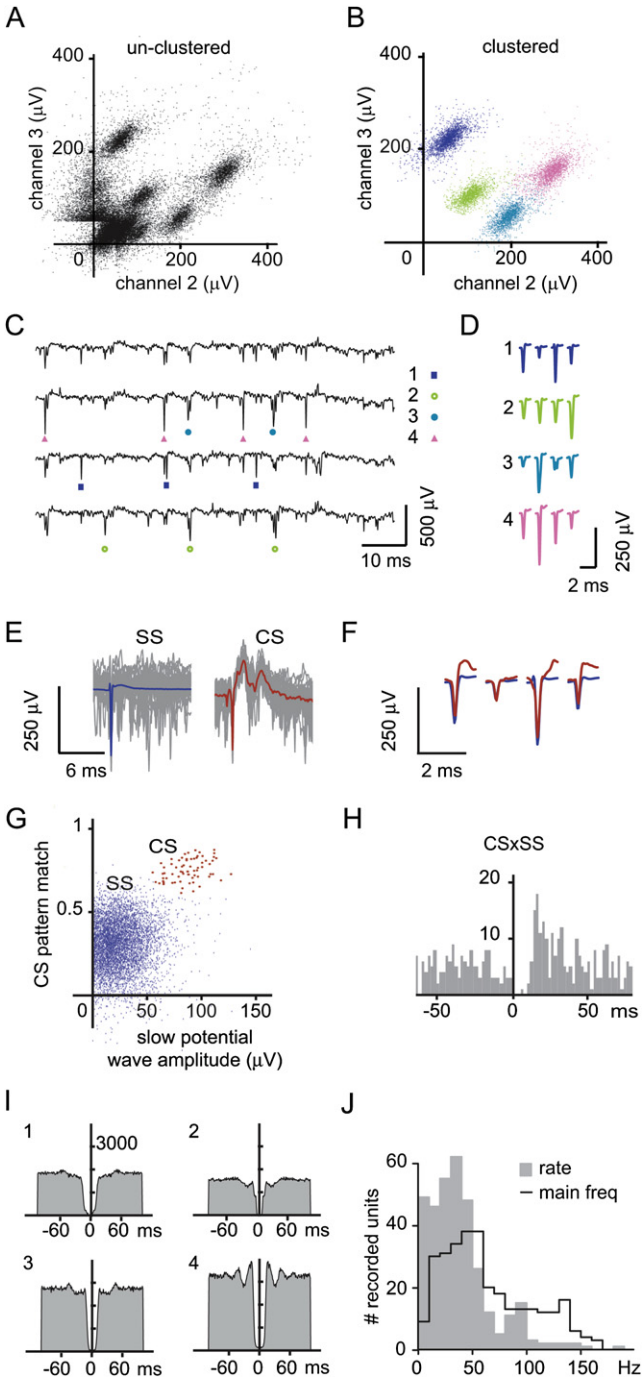

Figure 1. Simultaneous Recordings of Multiple Cerebellar Purkinje Cells with Tetrodes

(A and B) Example of a tetrode recording where four units were isolated. The scatter plots represent the peak amplitudes of spikes (threshold at 50 μV) on two channels of a tetrode. (A) Plot of unsorted spikes for 1 min of recording. (B) Same plot after assignment of spikes to four different units, represented by four different colors (unassigned spikes are not displayed).

(C) Raw traces of the four channels. The spikes belonging to the different units are indicated by color symbols under the channel on which they exhibit the largest amplitude. Note the occurrence of near-coincident spikes.

(D) Average (unfiltered) waveforms of the four units on the four channels.

(E–H) Isolation of complex spikes for a Purkinje cell (unit 1 from panel [A]). (E) Average (unfiltered) waveforms overlaid with 25 successive simple spikes (SS) or complex spikes (CS) on one channel. (F) Average waveform of simple spikes and complex spikes over the four channels of the tetrode, showing the similarity of the amplitude profile over the four channels of the initial spike of the complex spike and the simple spike. (G) The scatter plot (for 3 min recording) represents the amplitude of the slow wave after the spike obtained from low-pass-filtered (800 Hz) spikes ("slow potential wave amplitude") plotted against the Spearman correlation of the spike with the average waveform of 15 hand-isolated complex spikes from the unit ("CS pattern match"). (H) The crosscorrelogram between complex spikes and simple spikes shows the characteristic pause of the latter after the occurrence of complex spikes.

(I) Autocorrelograms of the four units in panel (B). Same y scale for the four plots.

(J) Mean discharge rate and frequency of the main autorhythmicity mode for 346 units (NB: for 27 units, none could be identified).

RESULTS

Tetrode Recordings in the Purkinje Cell Layer

To study the organization of cell firing in the cerebellar cortex, we performed tetrode recordings from the Purkinje cell layer of this structure (Figure 1). Clustering of extracellular spike waveforms typically enabled discrimination of three to seven units from a single tetrode (Figures 1A–1D, see Experimental Procedures). In addition to simple spikes, complex spikes, which are characteristic of climbing fiber activation of Purkinje cells, were routinely observed in the recorded units, but they could be properly isolated only for a subset of the units (typically one to three) (Figures 1E–1H).

The temporal properties of single-unit firing were compared to the known properties of Purkinje cells (e.g., Armstrong and Rawson, 1979; Cerminara and Rawson, 2004). Most units exhibited an autocorrelogram with a profound central trough, occasionally bordered by ripples, revealing varying degrees of autorhythmicity (Figure 1I), as has been previously reported for Purkinje cells in vivo and in vitro (Armstrong and Rawson, 1979; Hausser and Clark, 1997). These units had an average firing rate of 38.1 ± 30.2 Hz (n = 346, mean ± SD, Figure 1J) and a main peak in their spectrum, corresponding to their modal frequency, at 63.3 ± 39.6 Hz (mean ± SD, Figure 1J). The large difference between the unit firing rate and main peak in the spectrum results from the presence of pauses in cell firing (Armstrong and Rawson, 1979; Cerminara and Rawson, 2004; Loewenstein et al., 2005; Steuber et al., 2007). These pauses explained the large coefficient of variation of the interspike intervals of 1.20 ± 1.07 (mean ± SD, with a clear bimodal distribution, 12% of the sample having large coefficient of variation values in the range 2–10).

Another type of unit was also occasionally encountered. These units had flatter autocorrelograms than Purkinje cells, were devoid of complex spikes, and their firing was associated with a 5–10 ms reduction in Purkinje cell firing, suggesting that they might be interneurons. These units were not associated with the fast oscillations described below (unpublished data) and are not considered further in the present study.

Synchrony between Neighboring Purkinje Cells Associated with Fast Oscillations in the Purkinje Cell Layer

To test whether Purkinje cells fire in relation to one another, we computed their crosscorrelograms (Figure 2). These often

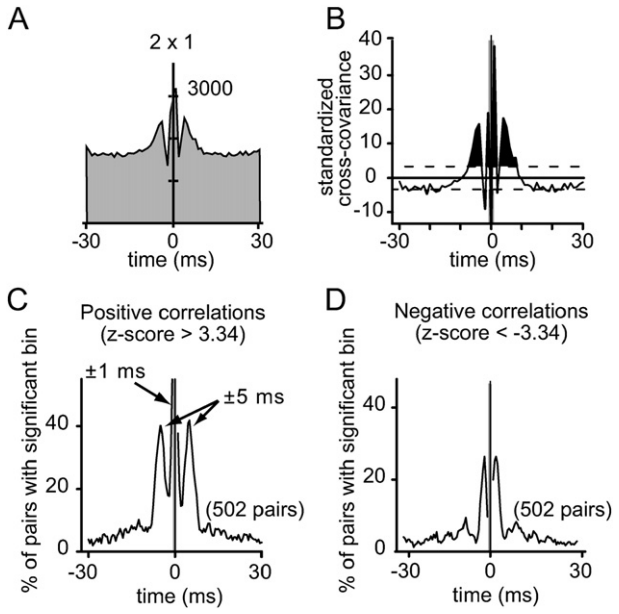

Figure 2. Short-Term Correlations between Purkinje Cells

(A) Crosscorrelogram of two neighboring Purkinje cells recorded simultaneously from a single tetrode (units 1 and 2 from Figure 1). The y axis corresponds to the count of events. See Experimental Procedures for the missing value at 0.

(B) Principle of identification of the bins with significant correlation in the standardized crosscovariance histogram (whose values are analogous to z scores). The dashed lines indicate the lower and upper limits of the confidence interval. Filled parts of the histogram indicate the presence of correlations departing significantly from the expectation for independent spike trains.

(C and D) Fraction of pairs with significant correlations for time bins between −30 and +30 ms. Positive correlations (C) and negative correlations (D) correspond to observed correlations larger and smaller than expected, respectively. Data from 502 pairs from 242 units with a firing rate above 10 Hz, from 61 recording sites in 45 rats.

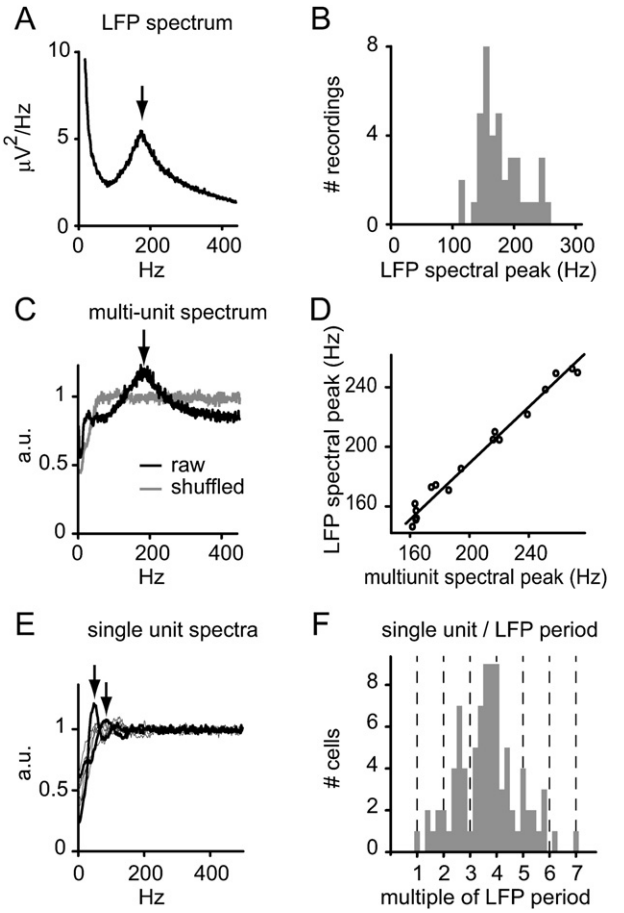

Figure 3. Multiunit Spike Discharge Is Organized at a High Frequency, which Is Observed in the Extracellular Field Potential

(A) Example of a spectrum of the local field potential (LFP) (the peak is marked by the arrow).

(B) Distribution of the high-frequency peaks in the LFP power spectra from 40 recording sites.

(C) Example of a peak at high frequency (200 Hz, black arrow) in the multiunit spectrum (raw, in black). The peak is absent in the disorganized multiunit activity (shuffled, in gray, see Supplemental Data). Same recording site as in (A).

(D) Correspondence between the peak frequencies in multiunit spike trains and the LFP. The scatter plot shows the peak frequencies for 17 recordings and a linear regression (slope = 0.94, r^2 = 0.98).

(E) Example of single-unit spectra ("single units"), which display peaks at lower frequencies than the LFP frequency (black traces and arrows correspond to two different units). Same recording site as (A).

(F) Individual cells do not oscillate at a subharmonic frequency of the LFP frequency. Distribution of the ratios of the periods of single Purkinje cell layer units (n = 92) and the corresponding periods of the LFP oscillations.

displayed a central peak, indicating the presence of synchronous (<2 ms) firing, associated with 5 ms side peaks (Figure 2A). To pool results from all unit pairs, we identified in the crosscorrelograms the bins where counts fell outside a confidence interval determined from the expectation for two independent spike trains (Figure 2B and see Supplemental Data). Eighty-five percent of all pairs showed significant correlation (n = 502 pairs from 242 cells firing above 10 Hz out of 292). Large fractions of significant positive correlations were found at ±1 ms, confirming the presence of synchrony (any peak at 0 ms could not be resolved, see Experimental Procedures). Further positive correlations at ±5–6 ms and negative correlations at ±2–3 ms (Figures 2C and 2D) were also observed in a large number of pairs (~40% and 25%, respectively). Units with a slow average firing rate (<10 Hz) only rarely exhibited significant correlations with their neighbors (n = 206 pairs with one slow unit from 48, data not shown). Thus, neighboring Purkinje cells express millisecond-scale synchrony together with a preferential firing at ~5 ms intervals, indicating of the presence of a fast (~200 Hz) rhythm.

The spectrum of the local field potential in the Purkinje cell layer revealed fast oscillations. In most (40/44) cases, a peak frequency greater than 100 Hz was fitted (see Supplemental Data). The peaks were distributed in the 120–260 Hz range (Figures 3A and 3B). Corresponding small-amplitude oscillations (typically tens to hundreds of microvolts) were occasionally visible in the raw traces, but were usually difficult to observe in the Purkinje cell layer because of the intense activity. One or a few oscillations could usually be seen in the spike-triggered average of the extracellular potential, with the spike riding on the negative phase of the wave (insets in Figure 6).

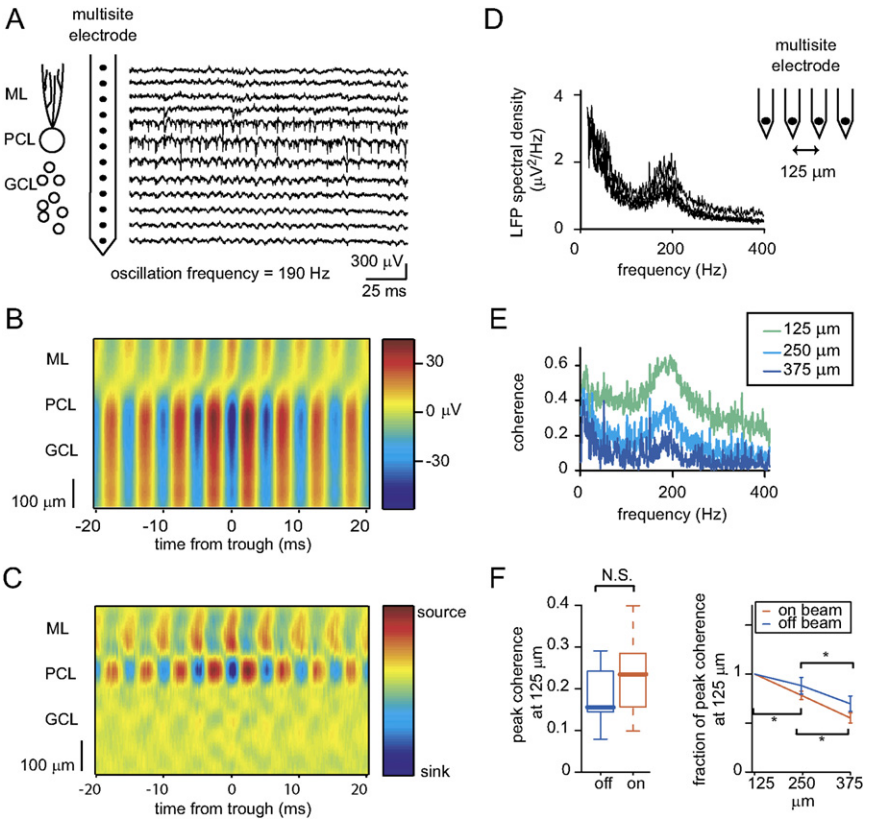

Figure 4. Spatial Extent of Fast Oscillations in the Extracellular Potential

(A) Example of simultaneous recordings across layers performed with a linear multisite electrode. The layers are indicated on the left (ML, molecular layer; PCL, Purkinje cell layer; GCL, granule cell layer).

(B) Wave-triggered average from the recording plotted in (A). The wave-triggered average of the raw signal (20 s recording) was triggered on the troughs of the filtered (150–230 Hz) signal. Note the phase inversion between the granule cell layer and the molecular layer. A linear interpolation over the y axis between the 15 channels has been performed for display purposes in panels (B) and (C).

(C) Current-source density analysis of the unfiltered signal from the example plotted in (A). This indicates that the pattern of potential displayed in (B) results from an alternating source-sink dipole between the Purkinje cell layer and the molecular layer. Such a pattern of alternating current sources-sinks was observed in 9 out of 11 experiments.

(D) Example of spectral density recorded from a multishank electrode with four recording sites parallel to the cerebellar surface along the parallel fibers and separated by 125 μm. Frequency and intensity of high-frequency oscillations in the extracellular potential are similar on the four recording channels.

(E) Example of spectral coherence as a function of distance, obtained from the same recording as in (D).

(F) (Left) Boxplot of peak coherence at 125 μm on parallel ("on beam") and orthogonal ("off beam") to the parallel fibers. (Right) Decrease of peak coherence as a function of distance in the two axes: "on beam" (along the parallel fibers, n = 15 recording sites from 9 rats) and "off beam" (in a parasagittal plane, n = 22 recording sites from 6 rats). Error bars correspond to SEM. The star (*) and "N.S." indicate significant and nonsignificant differences, respectively, between conditions or groups using the Wilcoxon rank test, $p < 0.05$.

To test whether the field potential oscillations were related to the correlation between neighboring Purkinje cells, we analyzed the spectral density of multiunit spike trains. When four or more units could be isolated in the Purkinje cell layer, single-unit spike trains were reunited in a multiunit spike train for spectral analysis. In these cases, a high-frequency peak was often present in the spectrum of the multiunit spike trains (a fitted peak >100 Hz; n = 17/28), revealing an emergent organization of the population at a high frequency (Figure 3C). The high-frequency peak in the multiunit spectrum was absent when the multiunit activity was disorganized by shifting independently the single-unit spike trains (Figure 3D, see Supplemental Data), demonstrating that the high-frequency peak depends upon correlations between units. The peak frequency in the multiunit spike train spectrum corresponded to the peak frequency in the extracellular spectrum (Figure 3D).

Because Purkinje cells tend to fire rhythmically (Figure 3E), we examined whether the main oscillatory mode of each cell was related to the global population oscillation. We compared the period of the main oscillatory mode of each cell to the period of the field oscillation (Figure 3F). If a cell fired every 2, 3, or any integer N cycles of the oscillation, the ratio between its period and the period of the field oscillation should be 2, 3, or N. However, the distribution of this ratio for a large number of cells did not exhibit peaks around integer values (Figure 3F, dashed lines), indicating that there was no systematic relation between the periods of single-unit oscillations and that of the field oscillation. Thus, the high-frequency peak does not depend upon intrinsic properties of single units (such as a harmonic of the main, lower, frequency of individual units).

These results demonstrate the existence of a high-frequency organization of cerebellar cortical activity, associated with a millisecond-scale synchrony of Purkinje cells, and that the peak in the spectrum of the extracellular potential in the Purkinje cell layer results, at least in part, from the multiunit coordination of discharge of Purkinje cells.

Field-Potential Oscillations Are Generated in the Purkinje Cell and Molecular Layers and Display Similar Coherence in the Transverse and Parasagittal Directions

To localize the currents generating the oscillations, we recorded simultaneously the extracellular potentials in the different layers of the cerebellar cortex, using linear silicon electrodes in penetrations orthogonal to the layers. High-frequency oscillations could be seen in all the layers (Figures 4A and 4B). The wave-triggered average of the local field potential displayed (Figure 4B) a uniform phase across the Purkinje cell and granule cell layers but a reversal of phase in the molecular layer. The amplitude of the oscillation was maximal in the Purkinje cell layer and

decreased with distance from the Purkinje layer. The spikes recorded in the Purkinje cell layer were phase locked to the negative phase of the oscillations in the granule cell layer (n = 6, phase = 198° ± 10° [mean ± SD], Figure S1). We then performed a current-source density analysis (Figure 4C), which revealed a source-sink pair in the Purkinje cell layer and the proximal molecular layer, indicating that the oscillations observed in the extracellular potential throughout the cerebellar cortex are generated in the layers containing the somata and proximal dendrites of the Purkinje cells.

To examine the lateral extent of the oscillations, we computed the spectral coherence of the extracellular field potential in a plane parallel to the surface. The oscillations were simultaneously recorded with four-shank electrodes (see Experimental Procedures) aligned either "on beam" (along the parallel fibers) or "off beam" (parasagittally). The spectral peak frequencies of the extracellular potential were the same on the four shanks (Figure 4D). Spectral coherence between shanks was observed over a broad range of frequencies, presumably reflecting the direct influence of current source/sinks, and decreased with distance (Figure 4E). However, a coherence peak at the oscillation frequency (the peak in the spectrum in Figure 4D) decreased more slowly with distance, and a small peak (~0.1) was generally still visible at the largest distance studied (375 μm), where broadband coherence was close to zero. The spatial decrement of oscillation coherence was independent of the orientation relative to the parallel fiber axis (Figure 4F). The high-frequency field-potential oscillations therefore exhibit coherence in the parasagittal and lateral directions over distances corresponding to at least ten Purkinje cell somata.

Pharmacological Agents that Uncouple Purkinje Cells from Their inputs Potentiate High-Frequency Oscillations

We then investigated the synaptic mechanisms underlying the oscillations. The first hypothesis we tested was that the fast Purkinje cell oscillations are driven by excitatory inputs, the parallel or climbing fibers (Bearzatto et al., 2006). In this case, a reduction of excitatory transmission should reduce the power of the oscillations, but intravenous administration of GYKI 52466 (Donevan and Rogawski, 1993), an antagonist of the AMPA receptors that mediate climbing and parallel fiber inputs to Purkinje cells (Konnerth et al., 1990), reversibly increased the oscillation power (3 ± 0.7-fold, p = 0.016, n = 7, Figures 5A, 5B, 5D, and 5E). Interestingly, the treatment did not alter the frequency of the oscillations (change in frequency: 0.22 ± 1.28 Hz, p = 0.94). The effective depression of the climbing fiber input by GYKI was verified by the complete disappearance of complex spikes (Figure 5C, GYKI: 99.7% ± 0.2% reduction of complex spike rate, p = 0.016). Thus, the oscillations do not require glutamatergic transmission to Purkinje cells. We confirmed that the oscillations did not require glutamatergic or other extracerebellar input by verifying the presence of oscillations after pedunculectomy (Figure S2).

The other fast neurotransmitter that could be responsible for high-frequency oscillations is GABA. We tested the effect of picrotoxin, a noncompetitive antagonist of GABA-A receptors, on the oscillations. Picrotoxin was injected shortly after GYKI injections, so that spurious glutamatergic activity resulting from the

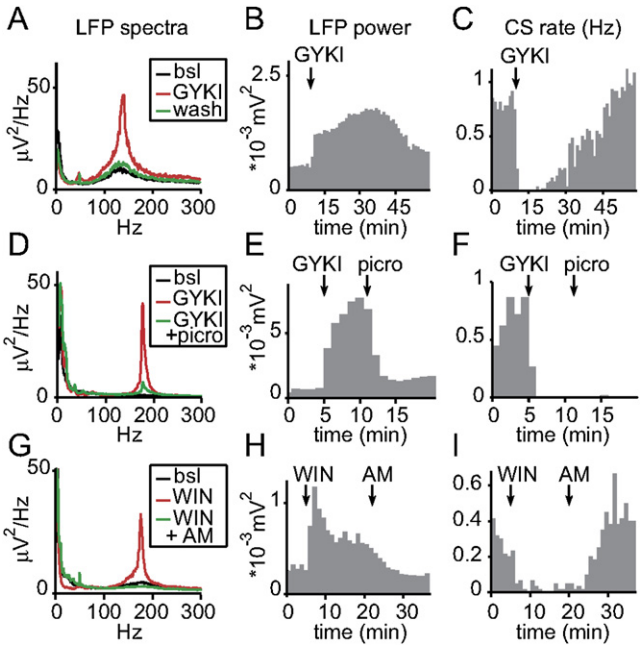

Figure 5. High-Frequency Oscillations Are Potentiated by AMPA Receptor Block (by GYKI 52466) or Cannabinoid CB1 Receptor Activation (by WIN 55,212-2), but Are Inhibited by GABA-A Receptor Block (by Picrotoxin)

Examples of the effects produced by the administration of the different pharmacological agents.

(A, D, and G) Spectra of the local field potential; each spectrum was calculated for 3 min of recording. (A) Spectra of the local field potential 5 min before ("bsl"), 3 min after ("GYKI"), and 50 min ("wash") after GYKI injection; (D) Spectra of the local field potential 5 min before ("bsl"), 3 min after GYKI injection ("GYKI"), and 1 min after picrotoxin injection ("GYKI + picro"). (G) spectra of the local field potential 5 min before ("bsl"), 3 min after WIN injection ("WIN"), and 10 min after AM 251 injection ("WIN + AM").

(B, E, and H) Time course of local field potential spectral power in a 50 Hz bandwidth around the oscillation frequency for the same three examples (bin = 1 min).

(C, F, and I) Evolution of complex spike rate for one Purkinje cell in each of the same three examples (bin = 1 min).

disinhibition of the cerebellum or external structures did not interfere with the oscillations (a nonsaturating concentration of picrotoxin was used, to avoid convulsions). Picrotoxin reduced the power of the high-frequency oscillations (Figures 5D and 5E, 37% ± 12% reduction, p = 0.031, n = 7) without restoring complex spikes (Figure 5F). Here also, the oscillation frequency was unchanged by picrotoxin (change in frequency: 4.87 ± 2.92 Hz, p = 0.16). These experiments indicate that GABAergic but not glutamatergic transmission is required for the genesis of the fast oscillations.

To investigate further the source of the synaptic inputs responsible for the oscillations, we applied the agonist of CB1 receptors WIN 55,212-2 (WIN), which acts presynaptically to suppress inhibitory inputs from local interneurons, together with excitatory inputs from climbing and parallel fibers (Levenes et al., 1998; Takahashi and Linden, 2000; Diana et al., 2002). This treatment should, however, preserve the GABAergic recurrent connections between Purkinje cells (Palay and Chan-Palay, 1974), because

they do not express CB1 receptors (Mailleux and Vanderhaeghen, 1992; Tsou et al., 1998). WIN (Figure 5G-I) induced a 4.14 ± 1.26-fold ($p = 0.0078$, $n = 8$) increase in the oscillation power and a 77% ± 3% ($p = 0.016$) reduction in complex spike rate. The strong increase in oscillation power was not accompanied by a change in frequency (−2.17 ± 4.01 Hz, $p = 0.84$). The effects of WIN were counteracted by the CB1 antagonist AM 251 ($n = 6$, Figures 5G–5I), which rescued complex spike firing (161% ± 63% of baseline firing rate) and yielded somewhat lower oscillation power than baseline (73% ± 9% of control, $p = 0.031$), suggestive of a constitutive activation of the CB1 receptors. Because WIN depresses excitatory and inhibitory inputs, we tested the action of WIN after the block of excitatory transmission by GYKI, in a separate set of experiments ($n = 6$). The injection of GYKI produced a 4.04 ± 0.81-fold ($p = 0.031$) increase, and the treatment with WIN further increased the oscillation power 1.21 ± 0.08-fold ($p = 0.031$). This indicates that WIN increases the oscillation power even after block of excitation and thus spares the GABAergic transmission responsible for the oscillations. In summary, our results suggest that the high-frequency oscillations are not driven by excitatory inputs but rather that they are mediated by cannabinoid-insensitive GABAergic synapses, most probably those of the recurrent collaterals of Purkinje cells.

We also examined the effect of the pharmacological treatments on the relation between Purkinje cell firing and the global oscillation. After block of AMPA receptors or activation of CB1 receptors, simple spikes remained time locked to the negative phase of the oscillations, while spike-triggered averages of the extracellular potential exhibited extended oscillations compared to control (Figure 6). We found no evidence for phase locking of complex spikes in spike-triggered averages. This and the strong oscillations observed during treatments blocking complex spikes suggest that climbing fibers are not entrained by the oscillations and play no role in their genesis. AMPA receptor block and CB1 receptor activation altered the firing of Purkinje cell layer units (Table 1), with a 15%–30% increase in the firing rate, a 5%–10% increase in the main firing frequency (the spectral peak in individual spike trains), and an enhancement of firing regularity, as evidenced by a 20% reduction of the coefficient of variation of the interspike intervals. These effects reflect an increased influence of the pacemaking activity of the Purkinje cells (Hausser and Clark, 1997) and may result indirectly from the disappearance of complex spikes (Cerminara and Rawson, 2004; Colin et al., 1980) or from the reduction of spontaneous inhibition. The increase in cell firing contrasts strikingly with the absence of any significant change in the frequency of the fast oscillations in the extracellular potential, showing that the high-frequency oscillation is remarkably independent of the features of single-unit firing.

High-Frequency Oscillations in a Network Model of Inhibitory Neurons Firing at Low Frequency

The above recordings established that Purkinje cell activity is organized in a high-frequency oscillation associated with precise synchrony between cells. The pharmacological profile of the oscillations indicated that an inhibitory (GABAergic) mechanism, most likely involving the recurrent Purkinje cell collaterals, underlies the oscillations. However, it was unclear whether this single mechanism could explain all our observations.

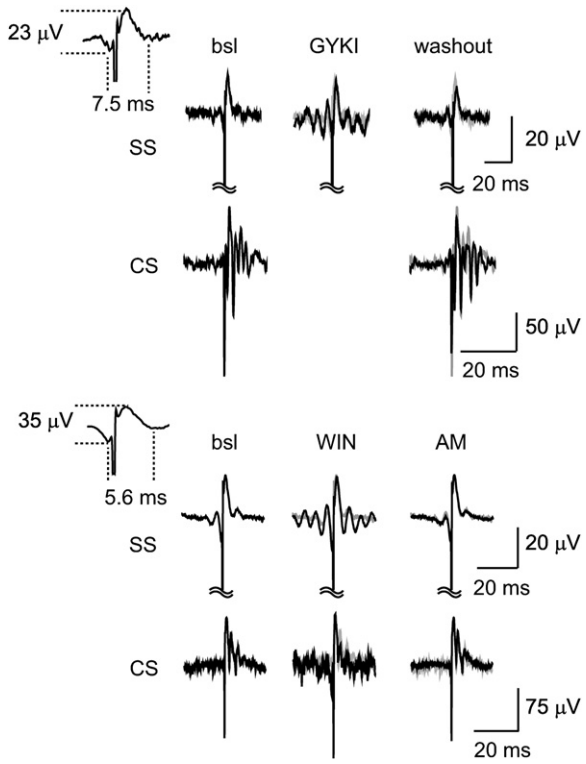

Figure 6. Examples of Spike-Triggered Averages under Control Conditions and after Potentiating the Oscillations by AMPA Receptor Block or Cannabinoid CB1 Receptor Activation

The spike-triggered average of the (unfiltered) local field potential was computed for the simple spikes (SS) and complex spikes (CS) of the same unit for baseline, drug GYKI 52466, or WIN 55,212-2 (WIN) and washout or AM 251. The baseline condition is overlaid in gray on the two other conditions. The inset (top left) is a close-up view of the simple spike in baseline condition showing one cycle of oscillation around the spike (the time interval indicated corresponds to the period of the LFP oscillation). Simple spikes were phase locked to the negative phase of the oscillations, while complex spikes were not. Only a few complex spikes could be detected in the presence of WIN, while there were none in the presence of GYKI.

Inhibition is known to be particularly effective at promoting zero-delay synchrony between neurons in population oscillations (Bartos et al., 2007). However, in most theoretical studies demonstrating fast oscillations in networks of inhibitory neurons (Wang and Buzsaki, 1996; Whittington et al., 1995; Maex and De Schutter, 2003), the inhibitory neurons fire at the oscillation frequency ("spike-to-spike synchrony"), which is not consistent with our data. Interestingly, model networks of simple single-compartment inhibitory neurons can operate in a dynamic regime in which neurons fire at low frequencies but nevertheless generate a high-frequency (>100 Hz) oscillation at the population level, with intermittent pairwise synchrony (Brunel and Hakim, 1999; Brunel and Wang, 2003). While these fast global oscillations resembled our observation, it remained to be determined whether such a regime would be consistent with the specific properties of our data: high-frequency oscillations, a wide spread of individual Purkinje cell firing rates, precise synchrony and strong damping of the oscillation in the crosscorrelogram,

Table 1. An AMPA Receptor Antagonist and a CB1 Receptor Agonist Increased the Firing Rate, the Frequency of the Main Autorhythmicity Mode, and the Regularity of Purkinje Cells

		Baseline		Treatment		
		Mean	SEM	Mean	SEM	p
WIN (n = 51)	Rate (Hz)	28.4	2.6	33.2	2.8	0.014
	Main Freq. (Hz)	48.4	3.0	52.6	2.9	0.017
	c.v. of isi	1.15	0.13	0.91	0.08	0.064
GYKI (n = 72)	Rate (Hz)	23.4	1.3	31.9	2.0	<0.001
	Main Freq. (Hz)	44.2	2.1	47.0	1.9	0.002
	c.v. of isi	1.12	0.16	0.89	0.09	0.005

The three parameters are the rate (average number of spikes/s), the main frequency (main peak in spectrum), and the coefficient of variation of the interspike intervals (irregularity of firing). The CB1 agonist WIN 55,212-2 and the AMPA receptor antagonist GYKI 52466 both significantly increased the rate and frequency of discharge and reduced the coefficient of variation of the interspike intervals. Numbers in parentheses correspond to the numbers of cells. There was no significant difference between the firing characteristics in the two baseline conditions (GYKI versus WIN experiments: p = 0.16, p = 0.33, p = 0.95 for rate, main frequency, and variation coefficient of interspike intervals, respectively).

very little influence of Purkinje cell rate on the frequency of the population oscillation, increase in power but not in frequency following reduction of the synaptic noise.

We set out to simulate these oscillations using a simplified model of the Purkinje cell network. A sparsely interconnected group of single-compartment Purkinje cells was modeled. The properties of the synaptic conductances were derived from our in vitro recordings (see below: rise time 0.5 ms, decay 3 ms, peak conductance 0.75 ns). Heterogeneity of firing rate was implemented by different depolarizing background currents, and their variation supplied the background synaptic noise (see Supplemental Data). In this initial model, the network activity showed little or no tendency to oscillate, unless the inhibitory conductances exceeded both reported values and our own measures (see below).

We therefore turned to a more realistic model of the Purkinje cell that included two separate compartments: a somatic compartment receiving recurrent GABAergic connections and a dendritic compartment receiving background synaptic noise. This separation endowed the soma with a short voltage time constant in response to current injection of ~0.1 ms. The partial isolation of the recurrent inhibitory inputs from the full dendritic capacitance of the Purkinje cell had two main effects. First, it allowed significantly higher oscillation frequencies to be attained (up to 300 Hz) than in the single-compartment model. Second, it reduced the required synaptic conductance by about 5-fold, allowing the network to generate oscillations at realistic conductance values (on the order of 1 ns). This model generated fast population oscillations over a wide range of parameter values (Figure 7). The model operated with the experimentally observed range of individual Purkinje frequencies (Figure 7D, compare with 1J) and interspike interval distributions. Synchrony between pairs of neurons was associated with damped oscillations in crosscorrelograms (Figure 7E, compare with Figure 2). The activity spectrum was reproduced in both control and low-noise conditions (mimicking the control conditions and the applications of GYKI/WIN, Figure 7F, compare to Figures 5A, 5D, and 5G). Finally, the reduction of noise levels strongly enhanced the oscillation power without altering their frequency, much as was observed during applications of GYKI/WIN.

We investigated the influence of various model parameters. The oscillation frequency was largely independent of Purkinje cell firing rate (Figure 7G) but strongly dependent on the synaptic latency, the inhibitory synaptic current rise time, and to a lesser extent on the synaptic decay (Figures 7H–7J) and conductance (Figure S3). These properties are in accord with previous studies of networks of single-compartment neurons (Brunel and Hakim, 1999; Brunel and Wang, 2003). Our simulation results were compared to an analytical calculation of the network frequency as a function of synaptic kinetics, under the assumption that the instantaneous firing rate of a single neuron follows oscillatory inputs with no phase shift at any frequency (see Supplemental Data). The two-compartment neurons exhibit a phase advance with respect to high-frequency oscillations, resulting in a network frequency systematically above the analytical prediction for single-compartment neurons.

In summary, a simple recurrent inhibitory model of the Purkinje cell network with sparse connectivity, noise levels, heterogeneity, and with a simplified two-compartment Purkinje cell geometry was able to reproduce the high-frequency oscillations and their observed pharmacological modulation.

Fast, Cannabinoid-Insensitive IPSCs in Mature Purkinje Cells

Most previous recordings of inhibitory postsynaptic currents (IPSCs) in Purkinje cells were performed in the developing cerebellum and yielded kinetics too slow to support high-frequency oscillations in our model: rise times of 1–3 ms and decay times of 10–20 ms (Konnerth et al., 1990; Vincent et al., 1992; Pouzat and Hestrin, 1997; Dean et al., 2003). We therefore measured IPSC kinetics in the mature cerebellum, by recording in slices from adult rats at near physiological temperature (Figure 8 and Supplemental Data). We studied both spontaneous IPSCs and IPSCs evoked by electrical stimulation in the molecular layer, likely from molecular layer interneurons. In the presence of the glutamate receptor antagonist NBQX, evoked IPSCs had a rise time of 0.41 ± 0.01 ms and a decay of 3.37 ± 0.88 ms (Figures 8A and 8B, n = 7). Spontaneous IPSCs (Figures 8A and 8C) were observed at a relatively high frequency (34 ± 7 Hz, n = 7), with an average amplitude of 36 ± 11 pA (in symmetric chloride, corresponding to ~0.6 ns). Most of these spontaneous events were due to presynaptic action potentials, because TTX application strongly reduced their frequency, by 86% ± 8% (n = 3). These spontaneous IPSCs exhibited somewhat faster rise times (0.25 ± 0.05 ms, $p < 0.01$) but similar decay times (3.16 ± 0.55 ms, p = 0.87) to the evoked IPSCs. These fast rise times suggest that most spontaneous IPSCs originated from synapses close to the soma, because dendritic inputs would have had longer rise times as a result of filtering (Roth and Hausser, 2001). These somatic IPSCs have rapid decay times, compatible with those required to obtain fast oscillations in our model.

Because strong oscillations were visible in the presence of the cannabinoid agonist WIN 55,212-2 in vivo, the IPSCs responsible

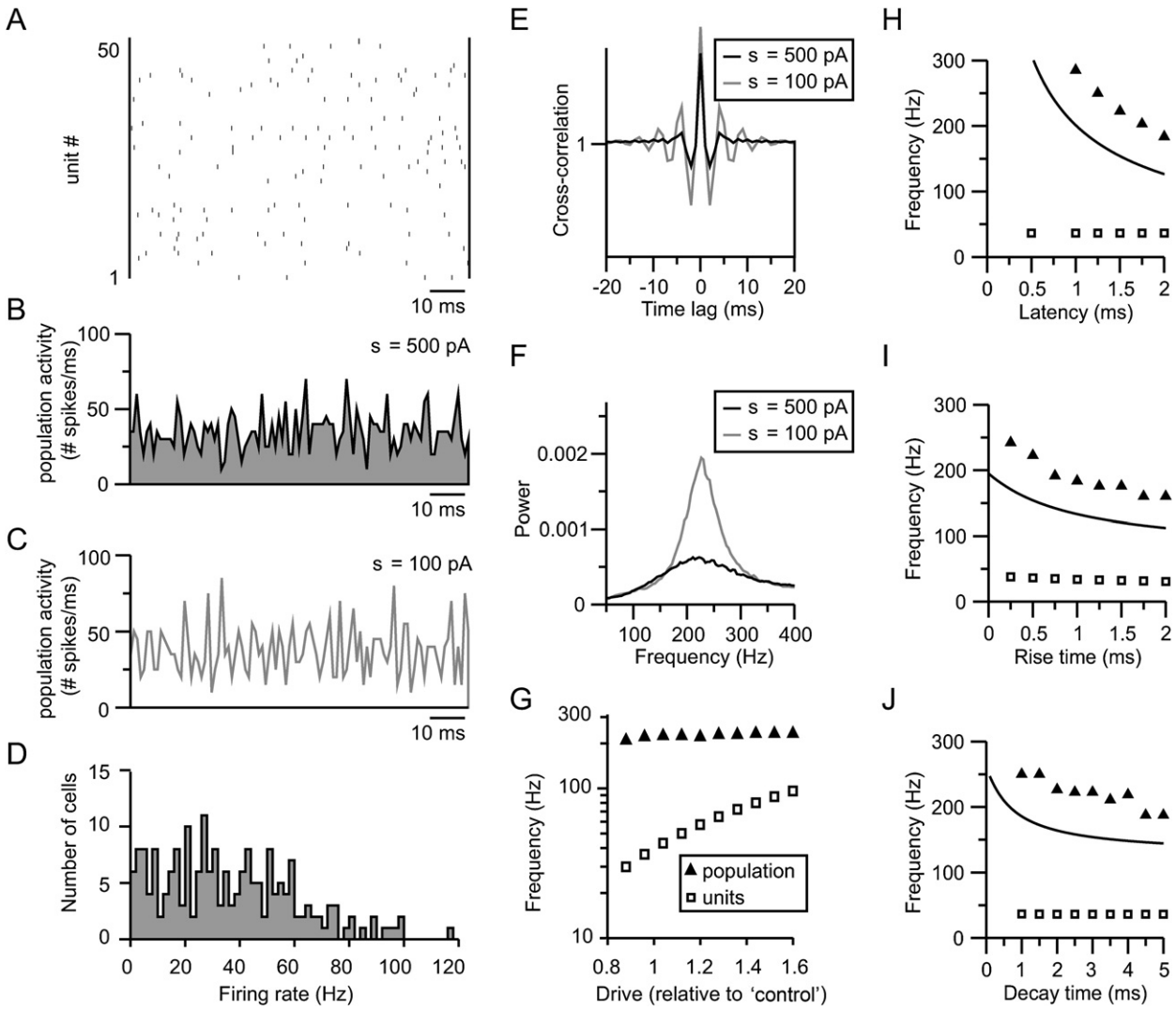

Figure 7. A Model Network of 200 Recurrently Connected, Heterogeneous Purkinje Cells Generates Oscillations that Are Similar to the Experimental Data

(A) Raster of 50 neurons during 100 ms of the simulation.

(B) Instantaneous population activity (number of spikes in 1 ms bins) for a large input noise. s indicates the standard deviation of the external noise. Same time period as panel (A).

(C) same as (B), for a smaller input noise (s).

(D) Histogram of single-cell mean firing rates.

(E) Crosscorrelation between pairs of cells, averaged over all pairs.

(F) Spectrum of global activity, for two different values of the input noise, indicated in the legend. Other parameters are indicated in Supplemental Data.

(G) The population oscillation frequency was not sensitive to changes in the mean firing rates of individual cells. The mean firing rate was changed by increasing the mean drive to all neurons in the network.

(H–J) The population oscillation frequency depended on the latency and the two synaptic time constants, as shown by varying one of these parameters while keeping the other two fixed at their reference value (latency = 1.5 ms, rise time = 0.5 ms, decay time = 3 ms): network frequency as a function of latency (H), of rise time (I), and of decay time (J). In (H)–(J), solid lines indicate an analytical prediction for a network of "ideal" neurons that follow oscillatory inputs with no phase shifts; filled triangles show population network frequency observed in simulations (location of peak in spectrum of global activity); open squares indicate the average single-unit frequency.

for the fast oscillations should be present in the presence of this drug. We therefore examined the effect of cannabinoid receptor activation on spontaneous and evoked IPSCs. WIN (n = 7) significantly reduced evoked IPSCs (61% ± 15% reduction, [mean ± SD], p = 0.015), an effect reversed by the antagonist AM 251 (n = 2). This result is consistent with the known depressant action of cannabinoids on interneuron-Purkinje transmission (Takahashi and Linden, 2000; Diana et al., 2002). In contrast, WIN (n = 9) did not induce significant changes in the frequency (80% ± 25% of baseline, p = 0.12), amplitude (85% ± 13% of baseline,

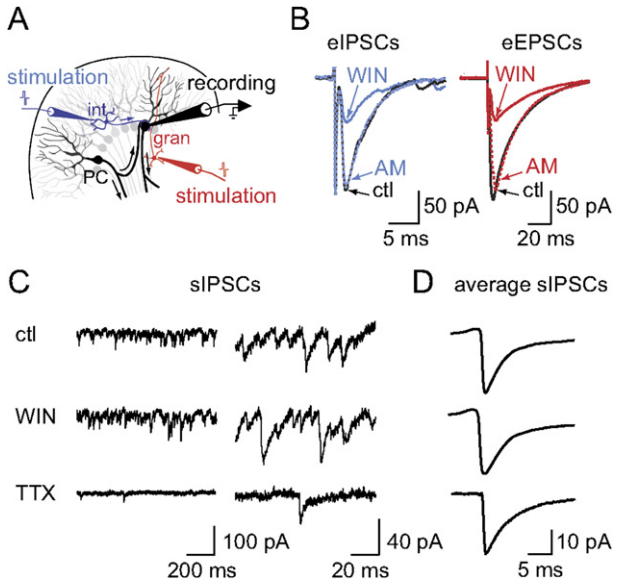

Figure 8. Fast Inhibitory Transmission in Purkinje Cells from Adult Rats

(A) Spontaneous and evoked inhibitory and excitatory postsynaptic currents (IPSCs and EPSCs) were recorded from Purkinje cells; IPSCs were evoked by stimulation in the proximal molecular layer (blue). EPSCs were evoked by stimulation in the granule cell layer (red) in separate experiments. Three presynaptic neurons connected to the recorded cell are represented: a molecular layer interneuron (int), a Purkinje cell (PC), and a granule cell (gran).

(B) (Left) Electric stimulation in the molecular layer (presumably of interneurons) evoked fast inhibitory synaptic currents (0.4 ms rise time and 3 ms decay) that were depressed by the cannabinoid agonist WIN 55,212-2 (WIN). Average of 30 sweeps. (Right) Electrical stimulation in the granule cell layer evoked excitatory synaptic currents (1.9 ms rise time and 16.9 ms decay) that were depressed by the cannabinoid agonist WIN. Average of 40 sweeps. The effect of WIN was reversed by the cannabinoid antagonist AM 251 (AM).

(C) The frequency and amplitude of the spontaneous inhibitory currents were not affected by the cannabinoid agonist WIN, and most IPSCs were suppressed by TTX. First and second columns: excerpt of the current trace at two different time resolutions.

(D) Average of the spontaneous synaptic events. These spontaneous synaptic events have fast time constants (rise time 0.25 ms, decay 3 ms), compatible with the requirements of our model (Figure 7). Experiments on IPSCs were performed in the presence of the AMPA receptor antagonist NBQX (10 μM). Experiments on EPSCs were performed in the presence of the GABA-A receptor antagonist picrotoxin (10 μM).

$p = 0.53$; an effect significantly smaller than that on evoked IPSCs, $p = 0.0006$) or kinetics (rise time: 100% ± 12% of baseline, $p = 1$; decay: 115% ± 7% of baseline, $p = 0.05$) of spontaneous IPSCs. Thus, most of the spontaneous, action potential-driven IPSCs did not originate from the CB1-sensitive interneuronal inputs, suggesting, moreover, that most interneurons are not spontaneously active in our preparation. These results demonstrate the presence in adult Purkinje cells of fast perisomatic IPSCs that are resistant to cannabinoids. The most likely source of these fast somatic CB1-insensitive IPSCs is the plexus of recurrent Purkinje cell axon collaterals.

Finally, we verified that WIN depressed excitatory synapses between granule cells and Purkinje cells (n = 6). WIN application reduced by 61% ± 22% (mean ± SD, $p = 0.031$) the amplitude of excitatory postsynaptic currents (EPSCs) evoked by stimulation in granule cell layer, an effect reversed by the antagonist AM 251 (n = 2).

High-Frequency Organization of Purkinje Cell Activity Is Present in the Unanesthetized Animal and Likely Arises from the Same Mechanisms as in Anesthetized Animals

To test whether the high-frequency oscillations were artificially induced by anesthesia, we also performed recordings in the Purkinje cell layer of freely moving (n = 2 rats) and head-restrained unanesthetized rats (n = 6 rats). Fast oscillations were observed in both preparations and were quantified in the head-restrained rats (22/31 recording sites). The peak frequency of the oscillations (254.2 ± 25.2 Hz, mean ± SD) was in the high range of frequencies observed in the anesthetized animals, and the spectral peak tended to be broader and of lower power (44% lower, $p = 0.002$ and 70% broader, $p < 10^{-4}$) compared to the anesthetized animals (Figures 9A and 9B). Millisecond-scale synchrony together with a preferential firing at ~4 ms intervals was found between neighboring Purkinje cells (Figures 9C–9F), corresponding to the ~250 Hz peak frequency found for the field potential oscillations in the unanesthetized animals.

We verified that the oscillations arose via the same mechanisms in unanesthetized and anesthetized animals by performing local injections of WIN at the sites of recording in head-restrained rats (n = 6 in 3 rats, see Supplemental Data). We observed a 6.2 ± 1.3-fold increase ($p = 0.03$) in the power of oscillations, with no change of frequency (−9.5 ± 3.4 Hz, $p = 0.06$, Figure 10), as observed in the anesthetized animal (Figure 5). Local injections of vehicle induced no clear change in the oscillation power (85% ± 32% of baseline, n = 4 in 3 rats). This indicates that high-frequency oscillations likely originate from the same mechanisms in unanesthetized and anesthetized animals.

DISCUSSION

We report that the activity of Purkinje cells is embedded in a population oscillation with a frequency several-fold greater than that of individual Purkinje cells. These oscillations are reflected in the field potential throughout the cerebellar cortex. Drugs that depress the excitatory and interneuronal inputs to the Purkinje cells, but presumably not their recurrent collaterals, potentiate these oscillations without altering their frequency. Simulations of recurrent networks of Purkinje cells reproduced multiunit oscillations similar in many respects to those we observed. Thus, our data finally provide an explanation for the high-frequency oscillatory phenomena first observed by Adrian in 1935 (Adrian, 1935).

Our results point clearly to the Purkinje cells as a major source of the oscillations in the extracellular potential. The primary feature of the oscillations is the synchronous discharge of neighboring Purkinje cells. The contribution of each Purkinje cell to the population oscillation remains elusive if each cell is considered in isolation, but the oscillations are visible in the spectral analysis of multiunit spike trains and in crosscorrelograms as ±5 ms side peaks. Interestingly, in the previous study of Bell and Grimm (1969) (its Figure 11), correlations at 5 ms were quite prominent but not mentioned. In the light of our results showing phase

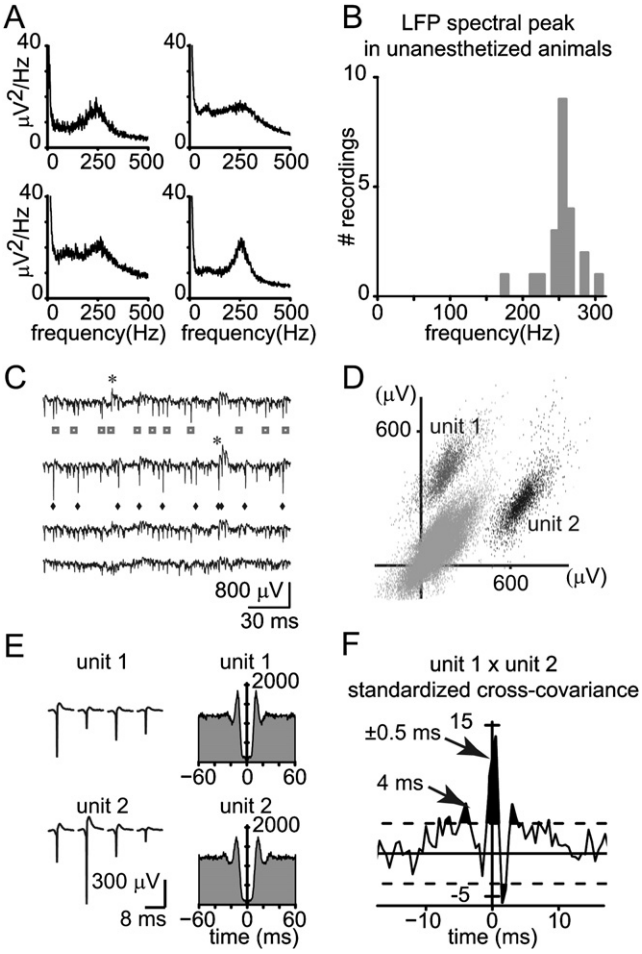

Figure 9. Local Field Potential Fast Oscillations and Short-Term Correlations between Neighboring Purkinje Cells Are Present in the Unanesthetized Head-Restrained Rat

(A) Example of spectra of the local field potential (LFP) of four recording sites in unanesthetized animals. The spectra were computed from 2 min of recording.

(B) Distribution of the high-frequency peaks in the LFP power spectra from 22 recording sites in 6 rats.

(C and D) Example of a tetrode recording where two Purkinje cells were isolated (same recording site as that used for the top-right spectrum in [A]). (C) Raw traces of the four channels. The spikes belonging to the different units are indicted by open squares and filled diamonds under the channel on which they exhibit the largest amplitude. Both simple and complex spikes (indicated by a *) are visible. (D) Scatter plot representing the peak amplitudes of spikes on two channels of the tetrode for 30 s of recording after assignment of spikes to the two units.

(E) (Left) Average unfiltered waveforms of spikes for the two units over the four channels. (Right) Autocorrelograms of the two units, bin = 1 ms.

(F) Standardized crosscovariance histogram for the same two units. Same legend code as in Figure 2B. Note the presence of significant correlations at ±0.5 and ±4 ms, indicating, respectively, synchronous firing and preferential firing at 4 ms intervals (corresponding to the 250 Hz peak frequency of local field potential oscillation). Bin = 0.5 ms.

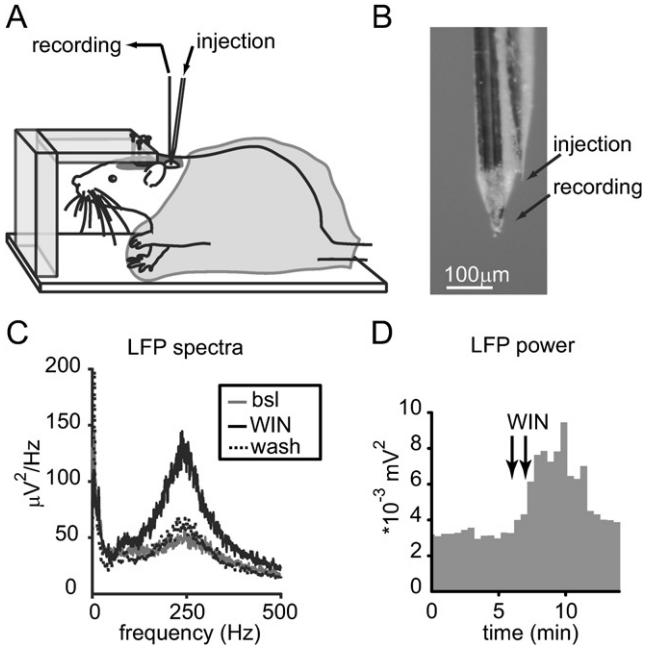

Figure 10. High-Frequency Oscillations in the Unanesthetized Animal Are Potentiated by Local Application of Cannabinoids

(A and B) Principle of the pharmacological experiment in the unanesthetized head-restrained animal. The animal's head was fixed by screws to the stereotaxic frame (A). A micropipette for pressure ejection was attached to the tetrode in order to eject the drug near the recording site (B).

(C and D) Example of the effect produced by the local ejection of WIN 55,212-2 (two pulses, 15 s, 30 psi). (C) spectra of the local field potential before ("bsl"') the ejections, 1 min after ("WIN"), and 5 min ("wash") after the ejections; each spectrum was calculated from 2 min of recording. (D) Time course of the local field potential spectral power in a 50 Hz bandwidth around the oscillation frequency (250 Hz) (bin = 30 s).

locking of the Purkinje cells to the oscillations and given the crucial role of fast inhibitory currents, the alternation of current source and sinks in the Purkinje cell layer may be interpreted as the result of the alternation of spikes (current sink) and inhibitory synaptic currents (current source) in the somata of Purkinje cells. The inverted pattern of currents in the molecular layer would then result simply from the passive return currents to the dendrites of the Purkinje cells. The oscillation coherence decreased over distances of a few hundred microns and showed no directional preference, contrary to the transverse preference that would have been expected if parallel fibers were entraining the oscillations. Thus, the oscillations emanate from networks of hundreds of Purkinje cells. Further evidence against a role for excitatory synapses comes from the increased power of the fast oscillations with block of AMPA receptors or stimulation of CB1 cannabinoid receptors, which strongly inhibit the excitatory inputs to the Purkinje cells (Levenes et al., 1998; Takahashi and Linden, 2000).

The reduction of the oscillations by picrotoxin indicates an important contribution of GABAergic neurotransmission to the genesis of the oscillations. The main inhibitory input to the Purkinje cells is provided by the molecular layer interneurons, but this input is strongly depressed by CB1 cannabinoid receptor activation (Takahashi and Linden, 2000; Diana et al., 2002). We confirmed this effect in adult rats on IPSCs evoked by stimulations in the molecular layer. CB1 receptor activation also blocked the parallel fiber EPSCs. However, we found that CB1 receptor

activation still increased (rather than decreased) the power of oscillation after the block of AMPA receptors. Molecular layer interneuronal inputs to Purkinje cells are thus unlikely to underlie the strong fast oscillations observed in the presence of a CB1 agonist. This conclusion is reinforced by our unpublished recordings of putative molecular layer interneurons in vivo, because these showed no correlation with the fast oscillations. Moreover, we showed that mature Purkinje cells receive cannabinoid-resistant IPSCs with fast kinetics, indicating a perisomatic origin (Roth and Hausser, 2001). Both the rise and decay times of these IPSCs fell in the range predicted by our model of fast oscillations. Therefore, a substantial fraction of somatic/perisomatic inhibition in adult Purkinje cells emanates from CB1-insensitive GABAergic terminals. These somatic inputs likely arise from the recurrent collaterals (Ramon y Cajal, 1911), which are particularly dense just below the Purkinje cell layer where they contact, among other targets, Purkinje cell somata (reviewed in Palay and Chan-Palay, 1974), and which should not be affected by CB1 cannabinoid agonists (Tsou et al., 1998; Mailleux and Vanderhaeghen, 1992). Recent direct recordings of Purkinje cell recurrent collateral inputs have been obtained in slices from young mice (Orduz and Llano, 2007; A.J. Watt et al., 2005, Monosynaptic inhibitory connections between pairs of Purkinje cells in mouse cerebellar cortex, Soc. Neurosci., abstract). The collaterals are myelinated and extend over hundreds of microns, with only a slight preference for the sagittal direction (Palay and Chan-Palay,1974; Bishop, 1982), which fits with our finding of a lack of directional preference in the coherence of oscillations and the symmetry of the 5 ms peaks in the Purkinje cell crosscorrelograms. In summary, our experiments indicate that recurrent inhibitory connections between Purkinje cells play a primary role in the genesis of the fast cerebellar oscillations.

Recent studies of high-frequency oscillations of hippocampal pyramidal cells have suggested that axonal gap junctions between principal cells are required to attain high frequencies of oscillation (Schmitz et al., 2001). However, no such junctions have been reported for Purkinje cell axons, and we found that the reduction of GABAergic transmission reduced the power of oscillations. We therefore sought to explain our results using only inhibitory synaptic transmission. Networks of recurrently connected inhibitory neurons are known to produce high-frequency oscillations (Wang and Buzsaki, 1996; Whittington et al., 1995; Maex and De Schutter, 2003; Bartos et al., 2007). In the regimes where the inhibitory neurons discharge at each cycle of the oscillation, such models require that the neurons receive sufficient excitation to sustain high frequencies, and under these conditions the network frequency is very sensitive to changes in inhibition (Wang and Buzsaki, 1996). The other known oscillatory regime of inhibitory networks, where cells do not fire at each cycle (Brunel and Hakim, 1999; Brunel and Wang, 2003), was closer to our data. However, whether such a regime could be attained for a network of cells with large dendritic trees (and therefore high capacitances), such as the Purkinje cells, remained to be established. We found it possible to generate fast oscillations in a network of simplified two-compartment Purkinje cells and to reproduce the main features of our results, namely: population oscillations in the correct frequency range, with similar statistics of cell discharge, crosscorrelations between cells, increase in oscillation power in response to a reduction of the input noise, and increase in cell firing rate without a change in the population oscillation frequency. Furthermore, we found that separating somatic and dendritic compartments allowed the network to oscillate at much higher frequencies, and with greater power, than occurred in networks of single-compartment neurons. This shows that recurrent connections between Purkinje cells are sufficient to explain the generation of the oscillations that promote synchrony of Purkinje cells without constraining their firing rate.

Interestingly, our model indicates that the main determinants for the oscillation frequency are the inhibitory synaptic delay and time constants (Brunel and Hakim, 1999; Brunel and Wang, 2003). Therefore, under conditions of intense cerebellar activity, it is conceivable that other inhibitory cell types than Purkinje cells contacted by Purkinje cells axons (such as Lugaro cells; Palay and Chan-Palay, 1974) or molecular layer interneurons (Laine and Axelrad, 1998; O'Donoghue et al., 1989) could be recruited in the oscillations, provided that the synaptic delays between the cell types were not too different from that between Purkinje cells. In these conditions, the oscillations would affect the feedforward inhibition mediated by molecular layer interneurons (Brunel et al., 2004) or the granule cell inhibition (via the Lugaro cell-Golgi cell connection; Dieudonne and Dumoulin, 2000) and thus constrain synaptic integration in the cerebellar cortex.

Finally, it should be noted that Purkinje cell axon collaterals tend to remain confined in zebrin compartments (Hawkes and Leclerc, 1989), presumably corresponding to functional modules. The axon collaterals undergo substantial remodeling during postnatal maturation of the cerebellum (Gianola et al., 2003), when reshaping and pruning could be guided by experience-dependent mechanisms. Recurrent inhibition could thus contribute, together with parallel-fiber-mediated excitation (Heck et al., 2007), to the synchrony of functionally related Purkinje cells (De Zeeuw et al., 1997). Convergence of this synchronized Purkinje cell activity should increase spike-timing precision in the target neurons in the deep cerebellar nuclei (Gauck and Jaeger, 2000). Although our experiments indicate the presence of fast oscillations (~250 Hz) in the cerebellar cortex of awake rats, in agreement with a previous report (Pellet et al., 1974), further multiunit recordings in awake animals during active behavior are required to understand better how short-term coordination of Purkinje cell firing contributes to cerebellar physiology.

EXPERIMENTAL PROCEDURES

Animals and Surgery

The Experimental Procedures were conducted in conformity with institutional guidelines and in compliance with national and European laws and policies. Experiments were performed on 67 anesthetized and 8 unanesthetized (see Supplemental Data) male adult Wistar Han rats (3–5 months old; 400–600 g; Charles River Laboratories, France). After the induction of anesthesia with a ketamine-xylazine mixture, the animal was mounted in a stereotaxic frame (David Kopf Instruments, CA) with bars in the ears and mouth and maintained anesthetized during the whole experiment with a mixture of isoflurane (0.5%–1.5%) and O_2. Twenty-two rats were administered with pharmacological agents (detailed below). For these studies, the femoral vein was catheterized to allow intravenous drug administration, and the trachea was cannulated to allow artificial respiration. Heart rate and blood O_2 concentration were monitored to adjust the level of anesthesia. A heating device controlled by rectal temperature

was used to maintain the rat at physiological core temperature. Before incision of the scalp, 3% lidocaine was injected subcutaneously at the site of incision. The skull and dura over the vermian part of lobules V and VIa were removed using a dental drill, a curved syringe needle, and fine forceps. Subdural meninges were gently removed where the electrodes were to be inserted. The surface of the cerebellum was maintained moist with a saline solution.

In Vivo Electrophysiology

Extracellular potentials were acquired with a Tucker Davis Technologies system3. Signals were referenced against a tungsten electrode positioned in saline at the surface of the cerebellar cortex. The signal from each channel was first filtered 0.1 Hz to 8 kHz with a Butterworth filter, then differentially amplified, sampled at 25 kHz, and stored to disk for off-line analysis. The activity was continuously monitored through loudspeakers and displayed on a computer screen monitor.

Simultaneous multiple single-unit recordings were obtained using the technique of tetrode recording (Wilson and McNaughton, 1993; Delescluse and Pouzat, 2006). Multiunit activity was recorded from the Purkinje cell layer (as determined by the presence of complex spikes) either with hand-made (12 μm Goodfellow Nickel-Chrome wires twisted together) or commercial tetrodes (Thomas Recording, tungsten electrodes in a quartz matrix) in the cerebellar vermis at depths ranging from 1 to 5 mm. Before recording, the tips of the wires were cleaned (Microelectrode Tip Cleaner, Thomas Recording) and gold-plated (gold solution, Sifco) to reduce their impedance to 200–300 kΩ. The tetrode was lowered in small increments of 10–50 μm. The different layers of the cerebellar cortex could be discriminated during the experiments according to their specific features. In particular, the Purkinje cell layer was characterized by an intense cellular activity and distinctive complex spikes (Figure 1E), while in the proximal molecular layer complex spikes appeared as 1–3 ms monophasic waves. The quality of discrimination did not seem to depend upon whether the Purkinje cell layer was approached from the molecular layer or the granule cell layer. The wide-band signal recorded by the tetrode is referred to as local field potential (LFP).

Multisite recordings for CSD and the spatial study of oscillations were obtained with linear probes of 16 electrodes arranged on one or four shanks (gift from the University of Michigan, available at NeuroNexus Technologies N2T). Recordings were obtained from lobule V or VIa. Probes were oriented in order to penetrate orthogonally to the lobule surface. In these experiments, LFP corresponds to the wideband signal on any channel of the probe.

Single-Unit Isolation

Continuous recordings were first high-pass filtered at 300 Hz with a Butterworth filter before thresholding (typically at 50 μV). Single-unit spikes were isolated off-line using either manual clustering ("xclust," M.A. Wilson) or semiautomatic clustering (Fee et al., 1996) (Matlab implementation by S.B. Mehta), using the peak amplitude or the amplitudes of five points around the peak. With these methods, three to seven units could be isolated per tetrode (Figures 1A and 1B). Neither of these procedures allowed the sorting of overlapping waveforms arising from coincident spikes from two or more different units, i.e., within an interval of less than 0.5 ms (the width of the Purkinje cells spikes being less than 0.3 ms). As a result, spike train crosscorrelations at submillisecond time-lag were not computed in this study. The accuracy of unit isolation was verified by confirming the existence of a 1–2 ms refractory period devoid of spikes in the autocorrelogram (Figure 1I). At this stage of the spike sorting, complex and simple spikes from a given unit were attributed to the same unit, because their initial spikes had similar amplitude profiles over all four channels (Figures 1F and S4). Complex spikes were discriminated on the basis of the presence of a slow component together with their stereotypical shape for a given Purkinje cell. The slow component was estimated from the low-pass-filtered (800 Hz) spike trace as the difference between the extrema of filtered potential in the 2.5 ms preceding and following the spike. Then, the resemblance with a stereotyped complex spike waveform was estimated by computing the Spearman rank order correlation coefficient of each spike waveform (for the 6 ms that followed the spike peak) with the average waveform of hand-selected complex spikes (n = 5–10) from individual units. The presence of a pause (20 ms or more) in simple spike firing of a Purkinje cell after a complex spike was verified. The stationarity of unit activity was controlled by calculating their average rate each second over the recording period.

Further analysis was performed with Matlab and GNU R (R Development Core Team, 2004).

Analysis of the Spatial Organization of Oscillations

Multisite recording for extracellular potential and current-source density (CSD) analyses were obtained with linear probes of 16 electrodes, with the probe perpendicular to the surface of the lobule. Wave-triggered averages were triggered on the minima of the signal filtered with a 0 lag 50 Hz band-pass Butterworth filter centered on the frequency of the fast oscillation peak in the power spectrum. Only minima whose amplitude were larger than 1.5 times the standard deviation of the filtered signal were used in the wave-triggered average. CSD analysis measures the distribution and amplitude of current sinks/sources in the extracellular medium (Nicholson and Freeman, 1975). In the present paper, we neglected the heterogeneity of conductivity in the extracellular medium, and the Laplacian of potential was approximated as its component along the axis perpendicular to the Purkinje cell layer, a reasonable approximation in the case of a laminar organization of sources and sinks of currents (Nicholson and Freeman, 1975). Therefore, the current source density I_m was approximated to $I_m \sim -s.d^2f/dz^2$, where s = conductivity, f = field potential, and z = axis orthogonal to the Purkinje cell layer. The mean CSD profile of the fast oscillations was derived by computing the CSD and forming from it a triggered average using the same trigger times as for the wave-triggered averages (see above).

The spatial coherence of oscillations was studied with four-shank linear silicon probes with shanks interspaced by 125 μm. The four shanks were either inserted along the parallel fiber beam ("on beam") or in the parasagittal plane ("off beam"), in the same lobule. Coherence between pairs of signals from different shanks was estimated with the Welch average periodogram method. Only one row of recording sites with similar spectral profile across shanks was used for each recording site. The four shanks thus yielded three estimates of coherence for signals recorded at a distance of 125 μm, two estimates for the distance of 250 μm, and one estimate for the distance of 375 μm. For a given recording site, the multiple estimates for a given distance were averaged. The characteristics of the peak in coherence were obtained from a fit with a Gaussian curve. Multiple recording sites in an animal belonged to different folds of the cerebellar cortex.

Pharmacological Study in Anesthetized Animals

All drugs (Tocris Cookson) were administrated intravenously (1 ml/min). This mode of administration was chosen in order to ensure a rapid onset of drug action, a reasonable control of the concentration of the drugs at the recording site, and an optimal stability of the recording. The drugs were dissolved in 1 ml vehicle containing 0.99 ml saline, 10 μl DMSO, and 100 mg hydroxypropyl-β-cyclodextrin for WIN 55,212-2 (WIN) and AM 251 or 200 mg hydroxypropyl-β-cyclodextrin for GYKI 52466 and picrotoxin. The dose of GYKI 52466 was 15 mg/kg, which has been shown to produce an ~80% inhibition of AMPA-mediated activity in the CA1 region of hippocampus (Mathiesen et al., 1998). The dose of WIN was 1 mg/kg, which produced the maximal reduction of locomotor activity in mice (Gifford et al., 1999). GYKI 52466 was injected in 20 animals. In seven of these animals, picrotoxin (4 mg/kg) was injected 6 min after GYKI, and in six animals WIN (1 mg/kg) was injected 10 min after GYKI. Eight animals were injected with WIN, of which six also received AM 251 (1 mg/kg). AM 251 was injected 15–40 min after WIN. In four animals, vehicle injection was verified to have no effect on simple or complex spike rates or on the power and frequency of the LFP oscillation. The drug effects were measured during periods of 3 min, taken 5 min before injection and 3 min after injection of GYKI, WIN, and picrotoxin.

Statistics

Values in the text are mean ± SEM, unless specified. Bivariate comparisons were performed using the one- or two-sample Wilcoxon rank tests, as appropriate.

SUPPLEMENTAL DATA

The Supplemental Data for this article can be found online at http://www.neuron.org/cgi/content/full/58/5/775/DC1/.

ACKNOWLEDGMENTS

This work was supported by the Centre National de la Recherche Scientifique (CNRS), the Institut National de la Santé et de la Recherche Médicale (INSERM, C.L.), the École Normale Supérieure (ENS), the European Commission (IST-2001-35271), the Ministère de la Recherche (ACI "Jeune Chercheur" and ACI "Neurosciences Intégratives et Computationnelles"), the Fondation Fyssen (G.S.), the Fondation pour la Recherche Médicale (C.S.), and the Agence Nationale pour la Recherche Neuroscience (ANR, OAC). The authors thank S.B. Mehta for sharing his spike sorting code and M.A. Wilson for sharing the Xclust software. C.d.S. thanks the MBL for the training provided by the Neuroinformatic course. We thank Ann Lohof and the UMR 7120 for help with pilot experiments. We thank Aline Stéphan, Jean-Marc Edeline, and Alain Péchard for their help with experiments in the unanesthetized animal.

Received: July 18, 2007
Revised: December 21, 2007
Accepted: May 7, 2008
Published: June 11, 2008

REFERENCES

Adrian, E. (1935). Discharge frequencies in the cerebral and cerebellar cortex. Proc. Phys. Soc. *83*, 32–33.

Armstrong, D.M., and Rawson, J.A. (1979). Activity patterns of cerebellar cortical neurones and climbing fibre afferents in the awake cat. J. Physiol. *289*, 425–448.

Bartos, M., Vida, I., and Jonas, P. (2007). Synaptic mechanisms of synchronized gamma oscillations in inhibitory interneuron networks. Nat. Rev. Neurosci. *8*, 45–56.

Bearzatto, B., Servais, L., Roussel, C., Gall, D., Baba-Aissa, F., Schurmans, S., de Kerchove d'Exaerde, A., Cheron, G., and Schiffmann, S.N. (2006). Targeted calretinin expression in granule cells of calretinin-null mice restores normal cerebellar functions. FASEB J. *20*, 380–382.

Bell, C.C., and Grimm, R.J. (1969). Discharge properties of Purkinje cells recorded on single and double microelectrodes. J. Neurophysiol. *32*, 1044–1055.

Bishop, G.A. (1982). The pattern of distribution of the local axonal collaterals of Purkinje cells in the intermediate cortex of the anterior lobe and paramedian lobule of the cat cerebellum. J. Comp. Neurol. *210*, 1–9.

Brookhart, J.M. (1960). The cerebellum. In Handbook of Physiology, Neurophysiology, J. Field and H.W. Magoun, eds. (Washington, DC: Am. Physiol. Soc.), pp. 1245–1280.

Brunel, N., and Hakim, V. (1999). Fast global oscillations in networks of integrate-and-fire neurons with low firing rates. Neural Comput. *11*, 1621–1671.

Brunel, N., and Wang, X. (2003). What determines the frequency of fast network oscillations with irregular neural discharges? I. Synaptic dynamics and excitation-inhibition balance. J. Neurophysiol. *90*, 415–430.

Brunel, N., Hakim, V., Isope, P., Nadal, J., and Barbour, B. (2004). Optimal information storage and the distribution of synaptic weights: perceptron versus Purkinje cell. Neuron *43*, 745–757.

Cerminara, N.L., and Rawson, J.A. (2004). Evidence that climbing fibers control an intrinsic spike generator in cerebellar Purkinje cells. J. Neurosci. *24*, 4510–4517.

Cheron, G., Gall, D., Servais, L., Dan, B., Maex, R., and Schiffmann, S.N. (2004). Inactivation of calcium-binding protein genes induces 160 Hz oscillations in the cerebellar cortex of alert mice. J. Neurosci. *24*, 434–441.

Cheron, G., Servais, L., and Dan, B. (2008). Cerebellar network plasticity: From genes to fast oscillation. Neuroscience *153*, 1–19.

Christian, K.M., and Thompson, R.F. (2003). Neural substrates of eyeblink conditioning: acquisition and retention. Learn. Mem. *10*, 427–455.

Colin, F., Manil, J., and Desclin, J.C. (1980). The olivocerebellar system. I. Delayed and slow inhibitory effects: an overlooked salient feature of cerebellar climbing fibers. Brain Res. *187*, 3–27.

De Zeeuw, C.I., and Yeo, C.H. (2005). Time and tide in cerebellar memory formation. Curr. Opin. Neurobiol. *15*, 667–674.

De Zeeuw, C.I., Koekkoek, S.K., Wylie, D.R., and Simpson, J.I. (1997). Association between dendritic lamellar bodies and complex spike synchrony in the olivocerebellar system. J. Neurophysiol. *77*, 1747–1758.

Dean, I., Robertson, S.J., and Edwards, F.A. (2003). Serotonin drives a novel GABAergic synaptic current recorded in rat cerebellar purkinje cells: a Lugaro cell to Purkinje cell synapse. J. Neurosci. *23*, 4457–4469.

Delescluse, M., and Pouzat, C. (2006). Efficient spike-sorting of multi-state neurons using inter-spike intervals information. J. Neurosci. Methods *150*, 16–29.

Diana, M.A., Levenes, C., Mackie, K., and Marty, A. (2002). Short-term retrograde inhibition of GABAergic synaptic currents in rat Purkinje cells is mediated by endogenous cannabinoids. J. Neurosci. *22*, 200–208.

Dieudonne, S., and Dumoulin, A. (2000). Serotonin-driven long-range inhibitory connections in the cerebellar cortex. J. Neurosci. *20*, 1837–1848.

Donevan, S.D., and Rogawski, M.A. (1993). GYKI 52466, a 2,3-benzodiazepine, is a highly selective, noncompetitive antagonist of AMPA/kainate receptor responses. Neuron *10*, 51–59.

Ebner, T.J., and Bloedel, J.R. (1981). Correlation between activity of Purkinje cells and its modification by natural peripheral stimuli. J. Neurophysiol. *45*, 948–961.

Fee, M.S., Mitra, P.P., and Kleinfeld, D. (1996). Automatic sorting of multiple unit neuronal signals in the presence of anisotropic and non-Gaussian variability. J. Neurosci. Methods *69*, 175–188.

Gauck, V., and Jaeger, D. (2000). The control of rate and timing of spikes in the deep cerebellar nuclei by inhibition. J. Neurosci. *20*, 3006–3016.

Gianola, S., Savio, T., Schwab, M.E., and Rossi, F. (2003). Cell-autonomous mechanisms and myelin-associated factors contribute to the development of Purkinje axon intracortical plexus in the rat cerebellum. J. Neurosci. *23*, 4613–4624.

Gifford, A.N., Bruneus, M., Gatley, S.J., Lan, R., Makriyannis, A., Volkow, N.D., Gifford, A.N., Bruneus, M., Gatley, S.J., Lan, R., et al. (1999). Large receptor reserve for cannabinoid actions in the central nervous system. J. Pharmacol. Exp. Ther. *288*, 478–483.

Hausser, M., and Clark, B.A. (1997). Tonic synaptic inhibition modulates neuronal output pattern and spatiotemporal synaptic integration. Neuron *19*, 665–678.

Hawkes, R., and Leclerc, N. (1989). Purkinje cell axon collateral distributions reflect the chemical compartmentation of the rat cerebellar cortex. Brain Res. *476*, 279–290.

Heck, D.H., Thach, W.T., and Keating, J.G. (2007). On-beam synchrony in the cerebellum as the mechanism for the timing and coordination of movement. Proc. Natl. Acad. Sci. USA *104*, 7658–7663.

Isope, P., Dieudonne, S., and Barbour, B. (2002). Temporal organization of activity in the cerebellar cortex: a manifesto for synchrony. Ann. N Y Acad. Sci. *978*, 164–174.

Konnerth, A., Llano, I., and Armstrong, C.M. (1990). Synaptic currents in cerebellar Purkinje cells. Proc. Natl. Acad. Sci. USA *87*, 2662–2665.

Laine, J., and Axelrad, H. (1998). Lugaro cells target basket and stellate cells in the cerebellar cortex. Neuroreport *9*, 2399–2403.

Levenes, C., Daniel, H., Soubrie, P., and Crepel, F. (1998). Cannabinoids decrease excitatory synaptic transmission and impair long-term depression in rat cerebellar Purkinje cells. J. Physiol. *510*, 867–879.

Loewenstein, Y., Mahon, S., Chadderton, P., Kitamura, K., Sompolinsky, H., Yarom, Y., and Hausser, M. (2005). Bistability of cerebellar Purkinje cells modulated by sensory stimulation. Nat. Neurosci. *8*, 202–211.

Maex, R., and De Schutter, E. (2003). Resonant synchronization in heterogeneous networks of inhibitory neurons. J. Neurosci. *23*, 10503–10514.

Mailleux, P., and Vanderhaeghen, J.J. (1992). Distribution of neuronal cannabinoid receptor in the adult rat brain: a comparative receptor binding radioautography and in situ hybridization histochemistry. Neuroscience *48*, 655–668.

Mathiesen, C., Varming, T., and Jensen, L.H. (1998). In vivo and in vitro evaluation of AMPA receptor antagonists in rat hippocampal neurones and cultured mouse cortical neurones. Eur. J. Pharmacol. *353*, 159–167.

Nicholson, C., and Freeman, J.A. (1975). Theory of current source-density analysis and determination of conductivity tensor for anuran cerebellum. J. Neurophysiol. *38*, 356–368.

O'Donoghue, D.L., King, J.S., and Bishop, G.A. (1989). Physiological and anatomical studies of the interactions between Purkinje cells and basket cells in the cat's cerebellar cortex: evidence for a unitary relationship. J. Neurosci. *9*, 2141–2150.

Orduz, D., and Llano, I. (2007). Recurrent axon collaterals underlie facilitating synapses between cerebellar Purkinje cells. Proc. Natl. Acad. Sci. USA *104*, 17831–17836.

Palay, S.L., and Chan-Palay, V. (1974). The Cerebellar Cortex: Cytology and Organization (New York: Springer-Verlag).

Pellet, J., Tardy, M.F., Dubrocard, S., and Harlay, F. (1974). Phasic electrical activity of the cerebellar cortex during sleep and wakefulness. Arch. Ital. Biol. *112*, 163–195.

Pouzat, C., and Hestrin, S. (1997). Developmental regulation of basket/stellate cell→Purkinje cell synapses in the cerebellum. J. Neurosci. *17*, 9104–9112.

R Development Core Team. (2004). R: A Language and Environment for Statistical Computing (Vienna, Austria: R Foundation for Statistical Computing), http://www.R-project.org.

Ramon y Cajal, S. (1911). Histologie du Système Nerveux de l'Homme et des Vertébrés. Vol. II (Paris: Maloine).

Raymond, J.L., Lisberger, S.G., and Mauk, M.D. (1996). The cerebellum: a neuronal learning machine? Science *272*, 1126–1131.

Roth, A., and Hausser, M. (2001). Compartmental models of rat cerebellar Purkinje cells based on simultaneous somatic and dendritic patch-clamp recordings. J. Physiol. *535*, 445–472.

Schmitz, D., Schuchmann, S., Fisahn, A., Draguhn, A., Buhl, E.H., Petrasch-Parwez, E., Dermietzel, R., Heinemann, U., and Traub, R.D. (2001). Axo-axonal coupling: a novel mechanism for ultrafast neuronal communication. Neuron *31*, 831–840.

Shin, S., and De Schutter, E. (2006). Dynamic synchronization of Purkinje cell simple spikes. J. Neurophysiol. *96*, 3485–3491.

Steuber, V., Mittmann, W., Hoebeek, F.E., Silver, R.A., De Zeeuw, C.I., Hausser, M., and De Schutter, E. (2007). Cerebellar LTD and pattern recognition by Purkinje cells. Neuron *54*, 121–136.

Takahashi, K.A., and Linden, D.J. (2000). Cannabinoid receptor modulation of synapses received by cerebellar Purkinje cells. J. Neurophysiol. *83*, 1167–1180.

Tsou, K., Brown, S., Sanudo-Pena, M.C., Mackie, K., and Walker, J.M. (1998). Immunohistochemical distribution of cannabinoid CB1 receptors in the rat central nervous system. Neuroscience *83*, 393–411.

Vincent, P., Armstrong, C.M., and Marty, A. (1992). Inhibitory synaptic currents in rat cerebellar Purkinje cells: modulation by postsynaptic depolarization. J. Physiol. *456*, 453–471.

Wang, X.J., and Buzsaki, G. (1996). Gamma oscillation by synaptic inhibition in a hippocampal interneuronal network model. J. Neurosci. *16*, 6402–6413.

Whittington, M.A., Traub, R.D., and Jefferys, J.G. (1995). Synchronized oscillations in interneuron networks driven by metabotropic glutamate receptor activation. Nature *373*, 612–615.

Wilson, M.A., and McNaughton, B.L. (1993). Dynamics of the hippocampal ensemble code for space. Science *261*, 1055–1058.